Design Study of Air-Core Coil Winding Topologies for Bearingless Axial-Force/Torque Motors

Walter Bauer
Johannes Kepler University
4040 Linz, Austria
walter.bauer@jku.at

Wolfgang Amrhein
Johannes Kepler University
4040 Linz, Austria
wolfgang.amrhein@jku.at

Abstract

The Bearingless Axial-Force/Torque Motor is a Lorentz-Force-Type actuator featuring a compact and integrated design using a special permanent magnet excitation system and a slotless air gap winding. The end-windings of the concentric air-core stator coils, shaped in circumferential rotor direction, provide active suspension forces in axial direction. The actuator unifies levitation force and drive torque generation in a single device unit sharing one common winding system. Especially for single-phase motor configurations, the resulting drive topology ensures the tilt stabilization of the rotor. In general, only a few air gap winding structures are suitable for proper polyphase drive torque generation without any negative side effects. The present article treats the drive torque and axial force generation mechanisms for Bearingless Axial-Force/Torque Motors and its influences regarding the appearance of tilt torques. As the radial drive stabilization is realized by multiple axial displaced passive magnetic ring bearings, the radial force generation due to a mismatch of the number of rotor pole pairs and the number of stator coils is also significant for drive stability considerations. As conclusion, numerical simulations for different drive configurations will prove for the validity of the presented analytical design framework.

1 Introduction

A bearingless drive is a motor with an integrated magnetic bearing (levitation) functionality, which allows the reduction of the number of necessary (additional) bearings. An important sub-category of such drives use one common winding system for levitation force and drive torque generation. The obtainable levitation forces in bearingless radial flux machines are usually radially directed. The fundamentals of this technology are well known and treated in [1], [2], [3] using the concept of different rotor and stator pole pairs for decoupled radial force and drive torque generation. The bearingless slice motor concepts presented in [4], [5] and [6] use passive reluctance forces of the back-iron for axial stabilization of the rotor disc together with one common winding system for radial suspension force and drive torque generation. In contrast to the above mentioned bearingless drives, the Axial-Force/Torque Motor presented for the first time in [7] and [8] is able to produce axial levitation forces and drive torques using only one common winding system.

1.1 Axial-Force/Torque Motor Technology - State of the Art

The suspension of a rigid rotor in three dimensional space requires the stabilization of six degrees of freedom (dof) either passively by constructive measures or by active control. The radial stabilization (2 dof) of the Axial-Force/Torque Motor is realized by repulsive magnetic forces of multiple interacting permanent magnet ring bearings mounted on rotor and stator. Since the ring bearings are axially shifted from each other, the tilting of the rotor (2 dof) is compensated as well. The passive magnetic suspension of 4 dofs causes a destabilization of the axial rotor direction. The end windings of the air-core stator coils can produce levitation forces in axial direction, provided that the rotor magnet system features a specific magnetization pattern. The special layout of the excitation

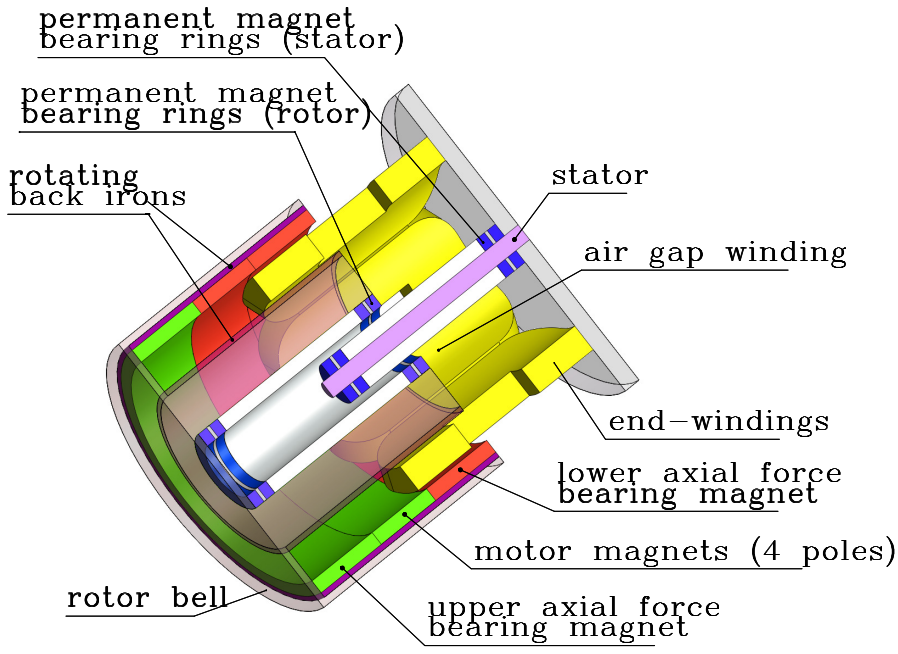

Figure 1: Presentation of the drive concept. State of the art single-phase Axial-Force/Torque Motor. Number of rotor pole pairs: $p_r = 2$. Number of air-core coils: $m = 4$. The bell-shaped rotor is axially shifted from its operating position.

system depicted in Figure 2 prevents the cancellation of the Lorentz Forces created by the coil end-windings. The current prototype [8] consists of an iron- and slotless stator ($m = 4$ stator coils) and a bell shaped, smooth rotor equipped with surface mounted permanent magnet blocks ($p_r = 2$ rotor pole pairs) located at the outer back-iron. Due to this highly symmetric drive configuration ($m = 4$, $p_r = 2$), the tilt torques caused by the end windings of the air-core coils annihilate each other. Unfortunately, the tilt stability of the current prototype configuration comes along with a disadvantageous single-phase motor characteristics.

1.2 Problem Statement

Obviously, drive configurations that feature a single-phase motor characteristics do not initiate additional tilt torques during drive torque and/or levitation force generation. In order to eliminate the detrimental single-phase motor behaviour, the next step in Axial-Force/Torque Motor development would be the systematic inclusion of the tilt torque generation mechanism into the drive analysis. The impact of drive torque and levitation force producing coil currents must be studied for polyphase windings. The extension of the single-phase Axial-Force/Torque Motor concept to polyphase winding structures requires also additional investigations regarding the appearance of perturbing radial forces. This turns out as important, since the radial stabilization of the rotor is ensured by passive magnetic ring bearings, which provides a very low mechanical damping. The present article is focused on the systematic search and selection of appropriate polyphase drive configurations for proper drive design without any unfavorable side-effects. The verification of the theoretical results

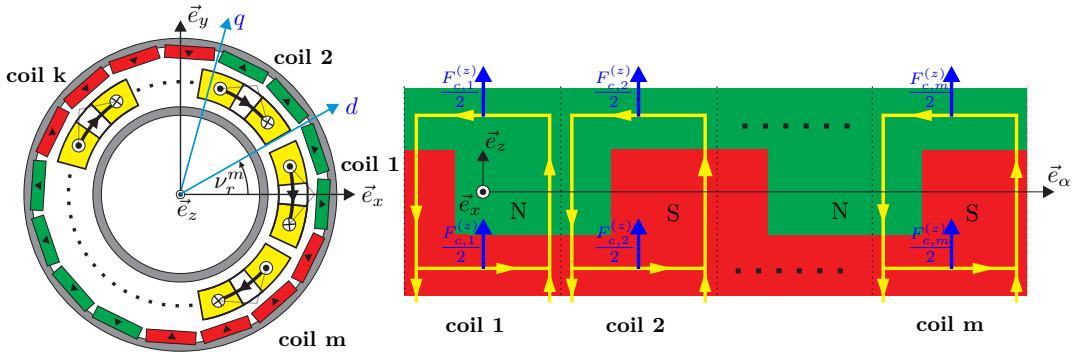

Figure 2: Polyphase air gap winding system of the Axial-Force/Torque Motor. Number of rotor pole pairs: $p_r = 2$. Definition of positive coil current directions.

by finite element analysis concludes the study.

2 Polyphase Air Gap Windings

The polyphase winding system of a Bearingless Axial-Force/Torque Motor (Figure 2) consists of m air-core stator coils (m phases). The coil axes are displaced at a mechanical angle of

$$\Delta\gamma_c = \frac{2\pi}{m} \tag{1}$$

from each other. The number of rotor pole pairs is denoted by p_r. Without loss of generality, the instantaneous current $i_{c,k}(t)$ of coil number k can be specified by

$$i_{c,k}(t) = i_F + \Re\left\{\underline{i}_T^{dq} e^{j\nu_r^e} e^{-j(k-1)p_r\Delta\gamma_c}\right\}, \tag{2}$$

where i_F denotes the axial (suspension) force generating current component and $\underline{i}_T^{dq}$ is the drive torque generating current phasor, which is a harmonic function of the electrical rotor angle ν_r^e.

$$\nu_r^e = p_r\Omega_m t + \nu_0^e\,. \tag{3}$$

As stated in (2), the generation of levitation forces in axial direction requires so called zero sequence coil current components i_F. Those components do not interfere with the drive torque generation mechanism of a set of balanced harmonic current components $\underline{i}_T^{dq}$.

3 Permanent Magnet Motor Excitation System

The radial flux density distribution $B_m(\gamma_r^e)$ of the motor magnet system at the air gap radius R_δ is given as a fourier series

$$B_m(\gamma_r^e) = \sum_{\substack{q=-\infty \\ \text{q odd}}}^{\infty} b_q e^{jq\gamma_r^e} \tag{4}$$

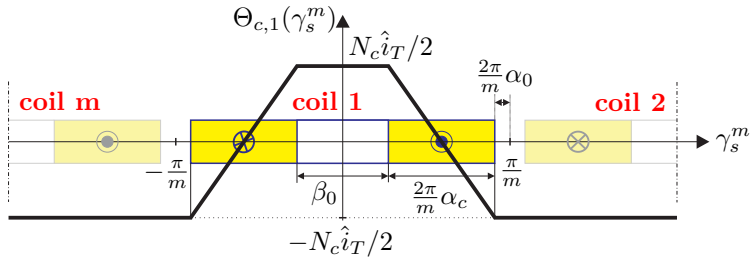

Figure 3: Calculation of the fourier series coefficients for a trapezoidal m.m.f. distribution of coil 1. Width of the coil core: $\beta_0 = \Delta\gamma_c(1-2\alpha_c-2\alpha_0)$.

of the electrical angular rotor coordinate γ_r^e. The transformation of (4) to mechanical stator coordinates γ_s^m using the transformations $\gamma_r^e = p_r\gamma_r^m$ and $\gamma_s^m = \gamma_r^m + \nu_r^m$ yields to

$$B_m(\gamma_s^m) = \sum_{\substack{q=1 \\ \text{q odd}}}^{\infty} \hat{B}_q \cos\left[qp_r\left(\gamma_s^m - \nu_r^m\right)\right] \tag{5}$$

with $\hat{B}_q = 2b_q$ denoting the q^{th} harmonic flux density magnitude of the motor magnet system. The radial flux density distribution is thus dependent on the mechanical stator coordinate γ_s^m and the rotor angle $\nu_r^m = \nu_r^e/p_r$.

4 Drive Torque Generation

The derivation of drive torque and radial force expressions for polyphase Axial-Force/Torque Motors require the definition of the linear current density $A^n(\gamma_s^m,t)$ of the air gap winding system. The distribution of the conductors and therefore also the distribution of the m.m.f. along the circumferential stator direction $\vec{e}_\alpha$ (mechanical angular variable: γ_s^m) is assumed as trapezoidal according to Figure 3. The m.m.f. $\Theta_{c,k}(\gamma_s^m,t)$ of the (single) coil number k of a m-phase winding system consisting of concentric, non-overlapping air-core coils is given as the fourier series

$$\Theta_{c,k}(\gamma_s^m,t) = \sum_{n=1}^{\infty} \frac{4}{\pi}\frac{N_c\xi_{w,n}}{2n} i_{c,k}\cos\Big(n\big(\gamma_s^m - (k-1)\Delta\gamma_c\big)\Big) + \frac{N_c i_{c,k}}{2\pi}\big(\Delta\gamma_c - \pi\big) \tag{6}$$

using the winding factor $\xi_{w,n}$ accounting for the effects of coil pitch and breadth. In case of a concentrated, m-phase winding system, the winding factor is determined by the simple expression

$$\xi_{w,n}^{conc} = \sin\big(n\frac{\Delta\gamma_c}{2}\big) = \sin\big(\frac{n}{m}\pi\big)\,. \tag{7}$$

The evaluation of the fourier series coefficients of the trapezoidal distributed m.m.f. depicted in Figure 3 gives (numerical) values for the winding factor (Figure 4) of a pitched and distributed air-core coil. The m.m.f. distribution of the air gap winding system results as the superposition

$$\Theta_a(\gamma_s^m,t) = \sum_{k=1}^{m}\Theta_{c,k}(\gamma_s^m,t) = \sum_{n=1}^{\infty}\Theta_a^n(\gamma_s^m,t) \tag{8}$$

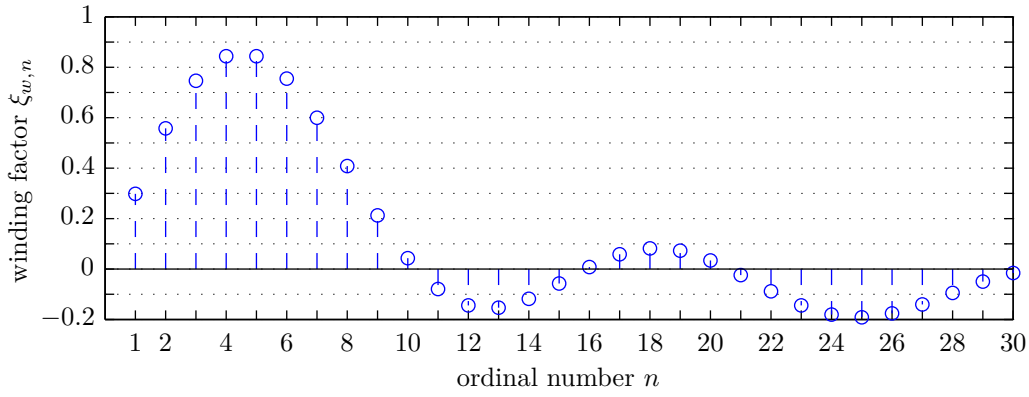

Figure 4: Winding factors $\xi_{w,n}$ for the trapezoidal m.m.f. distribution of Figure 3. Number of air-core coils: $m = 6$. Coil geometry data: $\alpha_0 = 0.0199$, $\alpha_c = 0.378$.

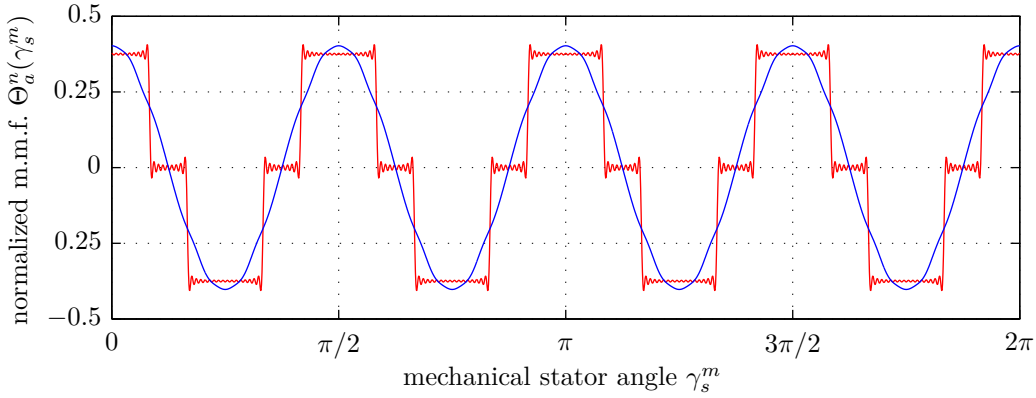

Figure 5: Normalized m.m.f. distribution $\Theta_a^n(\gamma_s^m)/(N_c\hat{\imath}_T)$ of a polyphase air gap winding consisting of air-core coils. Comparison between concentrated and distributed coils shown for $m = 6$, $\alpha_0 = 0.0199$, $\alpha_c = 0.378$ and $p_s = 4$ stator pole pairs. The first 100 harmonics of (8) are included.

of m single coil m.m.f. expressions (6) using a set of balanced, harmonic coil currents

$$i_{c,k} = \hat{\imath}_T \cos\Big(\omega_s t + \varphi_i - p_s(k-1)\Delta\gamma_c\Big) \tag{9}$$

without any zero sequence components. The (homopolar) offset component of the fourier series expression (6) is annihilated and therefore neglected for further considerations. After extensive derivations and simplifications, the geometrical harmonics of (8) can be stated as

$$\Theta_a^n(\gamma_s^m,t) = \frac{m}{\pi}\frac{N_c\xi_{w,n}}{n}\hat{\imath}_T \cdot \begin{cases} \cos(\omega_s t + \varphi_i + n\gamma_s^m), & \text{if } n = mz - p_s \text{ and } z \in \mathbb{N}; \\ & \text{(backward rotating wave)} \\ \cos(\omega_s t + \varphi_i - n\gamma_s^m), & \text{if } n = mz + p_s \text{ and } z \in \mathbb{N}_0; \\ & \text{(forward rotating wave)} \\ 0 & \text{else.} \end{cases} \tag{10}$$

in accordance with the deductions in [9]. An illustration of the rotating m.m.f. waves of a m-phase winding system reproducing a magnetic field with p_s pole pairs is shown in Figure 5. Based on (10), Table 1 can be used to explain the appearance or suppression of radial forces and/or certain m.m.f. harmonics during drive torque generation, see also section 5.

	$m=4$				$m=5$						$m=6$					
	$p_s=2$		$p_s=3$		$p_s=2$		$p_s=3$		$p_s=4$		$p_s=2$		$p_s=3$		$p_s=4$	
z	fw	bw	fw	bw	fw	bw	fw	bw	fw	bw	fw	bw	fw	bw	fw	bw
0	**2**		**3**		**2**		**3**		**4**		**2**		**3**		**4**	
1	**6**	**2**	7	1	7	3	8	2	9	1	8	4	**9**	**3**	10	2
2	**10**	**6**	11	5	12	8	13	7	14	6	**14**	**10**	**15**	**9**	16	8
3	**14**	**10**	**15**	**9**	17	13	18	12	19	11	20	16	**21**	**15**	22	14
4	**18**	**14**	19	13	**22**	**18**	23	17	24	16	**26**	**22**	**27**	**21**	**28**	**20**
5	**22**	**18**	23	17	27	23	28	22	29	21	32	28	**33**	**27**	34	26
6	**26**	**22**	**27**	**21**	32	28	**33**	**27**	34	26	**38**	**34**	**39**	**33**	40	32
7	**30**	**26**	31	25	37	33	38	32	39	31	44	40	**45**	**39**	46	38
8	**34**	**30**	35	29	**42**	**38**	43	37	**44**	**36**	**50**	**46**	**51**	**45**	**52**	**44**
9	**38**	**34**	**39**	**33**	47	43	48	42	49	41	56	52	**57**	**51**	58	50

Table 1: Generation of rotating fields. Arising m.m.f. harmonics of polyphase air gap windings. The table contains ordinal wave numbers n (mechanical coordinates). fw: forward rotating wave $n = mz + p_s$. bw: backward rotating wave $n = mz - p_s$. Red boxes: radial disturbance forces present. Yellow boxes: single phase motor characteristics. Green boxes: favorable configurations. The bold numbers denote the significant wave numbers for drive torque generation.

4.1 Interpretation of Table 1.

Drive torque generation. Steady state synchronous drive torques are generated by substitution of (12) and $p_s = p_r$ into (9). In case, that the appearing wave numbers of the forward and backward rotating field for a specific drive configuration of Table 1 are identical, an alternating field is created. This results in a single phase characteristics in terms of drive torque generation.

Appearance of radial forces. A (forward or backward) rotating field created for drive torque generation may provoke rotor angle dependent radial forces, if in addition to the drive torque generating wave number p_r one of the wave numbers $p_r \pm 1$ is also present in the m.m.f. spectrum of the considered configuration.

Tilt torque generation. A (forward or backward) rotating field created for drive torque generation provokes rotor angle dependent tilt torques in case, that the wave numbers given in Table 2 are also present in the corresponding m.m.f. spectrum of the considered configuration in Table 1.

4.2 Drive Torque Expression via Lorentz-Force Equation

The restriction of the general expression (8) to fundamental, forward rotating waves ($n = p_s$) yields

$$\Theta_a^{p_s}(\gamma_s^m, t) = \frac{m}{\pi}\frac{N_c \xi_{w,p_s}}{p_s}\hat{\imath}_T \cos(\omega_s t + \varphi_i - p_s\gamma_s^m)\,. \tag{11}$$

Higher harmonics of the m.m.f. spectrum of the air gap winding are neglected for drive torque analysis. The restriction to forward rotating fields implies $\omega_s t + \varphi_i - p_s\gamma_s^m = \text{const.}$ for the argument of the harmonic function in (11). The required electrical frequency for the coil currents in (9) is found by differentiation of the argument.

$$\omega_s = p_s\frac{d\gamma_s^m}{dt} = p_s\Omega_m\,. \tag{12}$$

The general relation between the n^{th} harmonic component of the linear current density (electric loading) and the causing m.m.f. distribution is given by

$$A^n(\gamma_s^m, t) = -\frac{1}{R_\delta}\frac{d\Theta_a^n}{d\gamma_s^m}\,. \tag{13}$$

The linear current density distribution of the forward rotating waves, producing p_s stator pole pairs, can be formulated using (13) together with (8) and (10).

$$A_{fwd}(\gamma_s^m, t) = \sum_{\substack{n'=\frac{m}{p_s}z+1 \\ z\in\mathbb{N}_0;\, n'\in\mathbb{Z},\, n' \text{ odd}}} -\frac{m}{\pi}\frac{N_c\xi_{w,n'p_s}}{R_\delta}\hat{\imath}_T \sin(\omega_s t + \varphi_i - n' p_s\gamma_s^m) \tag{14}$$

The fundamental component ($q = 1$) of the radial excitation flux density distribution (5) is given as

$$B_m(\gamma_s^m) = \hat{B}_1 \cos\left[p_r\gamma_s^m - p_r\nu_r^m\right] \tag{15}$$

using a description in mechanical stator coordinates γ_s^m and $\hat{B}_1 = 2b_1$. The calculation of the tangential Lorentz Forces caused by the axial directed conductor sections of the air gap winding requires the first (fundamental) wave ($n' = 1$) of the linear current density (14) distribution of the winding system

$$A_{fwd}(\gamma_s^m, t) = \hat{A}_{p_s} \sin\left[p_s\gamma_s^m - (\omega_s t + \varphi_i)\right] \tag{16}$$

with the amplitude $\hat{A}_{p_s} = \frac{m}{\pi}\frac{N_c\xi_{w,p_s}}{R_\delta}\hat{\imath}_T$. Based on a differential description of the stator forces

$$d\vec{F}_s = \left[A_{fwd}(\gamma_s^m)R_\delta d\gamma_s^m l_m\vec{e}_z\right] \times \left[B_m(\gamma_s^m)\vec{e}_\rho\right] \tag{17}$$

the drive torque expression is derived by evaluation of the vector cross product

$$d\vec{T}_s = \vec{r} \times d\vec{F}_s = (R_\delta\vec{e}_z) \times d\vec{F}_s\,. \tag{18}$$

The definitions of the reference frames and the force directions are depicted in Figure 6. The integration of (18) along the circumferential mechanical stator coordinate direction γ_s^m

$$\vec{T}_s = -R_\delta^2 l_m \int_0^{2\pi} A_{fwd}(\gamma_s^m)B_m(\gamma_s^m)d\gamma_s^m\,\vec{e}_z \tag{19}$$

results in an expression for the total drive torque

$$T_s^z = \begin{cases} -R_\delta^2\pi l_m\hat{A}_{p_s}\hat{B}_1 \sin\left(\nu_0^e - \varphi_i\right) & \text{if } \boxed{p_s = p_r}\,; \\ 0 & \text{else.} \end{cases} \tag{20}$$

acting on the stator winding system, which is in full accordance with [10].

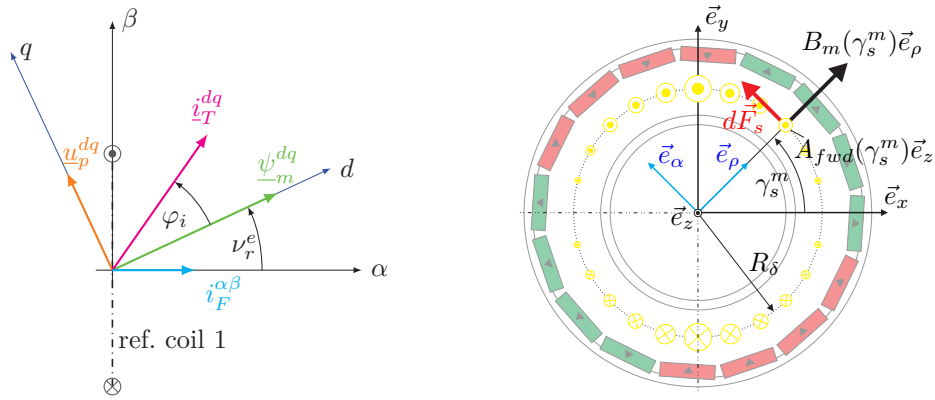

Figure 6: Definition of the linear current density of a forward rotating wave $A_{fwd}(\gamma_s^m)$. Drive torque and radial force calculation. Number of rotor pole pairs: $p_r = 2$.

5 Radial Force Generation

The appearance of radial forces during polyphase drive torque generation is especially undesirable for Bearingless Axial-Force/Torque Motors, as the radial rotor suspension is realized via passive magnetic ring bearings. The radial excitation flux density component depicted in Figure 6 can be transformed into a cartesian stator reference frame yielding

$$\vec{B}_m = B_m(\gamma_s^m)\vec{e}_\rho = B_m(\gamma_s^m)\left[\cos\gamma_s^m\vec{e}_x + \sin\gamma_s^m\vec{e}_y\right]. \tag{21}$$

The Lorentz Forces acting on the stator winding system of the drive are calculated by integration of (17) using the substitution (21) as well as (16) and (15).

$$\vec{F}_s = R_\delta l_m \int_0^{2\pi} A_{fwd}(\gamma_s^m, t) B_m(\gamma_s^m)\left[-\sin\gamma_s^m\vec{e}_x + \cos\gamma_s^m\vec{e}_y\right] d\gamma_s^m \tag{22}$$

The symbolic evaluation of integral (22) using the orthogonality relations of harmonic functions leads to very simple and descriptive radial stator force expressions for the $\vec{e}_x$-component

$$F_s^x = \begin{cases} \mp 2Q\cos\left[p_r\nu_r^m - (\omega_s t + \varphi_i)\right] & \text{if } \boxed{p_s = p_r \pm 1}\,; \\ 0 & \text{else.} \end{cases} \tag{23}$$

and the $\vec{e}_y$-component

$$F_s^y = \begin{cases} 2Q\sin\left[p_r\nu_r^m - (\omega_s t + \varphi_i)\right] & \text{if } \boxed{p_s = p_r \pm 1}\,; \\ 0 & \text{else.} \end{cases} \tag{24}$$

using the abbreviation

$$Q = \hat{B}_1 m N_c \xi_{w,p_s} l_m \hat{\imath}_T\,. \tag{25}$$

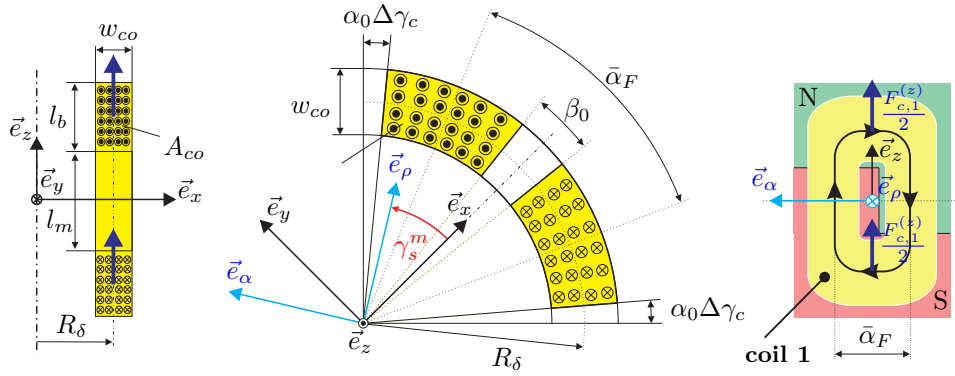

Figure 7: Generation of axial forces. Definition of the coil geometry. $\bar{\alpha}_F$: average end winding angle.

6 Generation of Lorentz Forces in Axial Rotor Direction

The resulting Lorentz forces of an arrangement of N_c single conductors in an external magnetic field, all bent and aligned in the same (circumferential) direction $\vec{e}_\alpha$ with an average conductor length of $\vec{l}_c = \bar{l}_c \vec{e}_\alpha$, each carrying the coil current $i_{c,k}$, can be calculated using

$$\vec{F}_{c,x} = (N_c i_{c,x})\, \vec{l}_c \times \vec{B}_\delta^F (w_m, w_\delta) \,, \tag{26}$$

where $\vec{B}_\delta^F = \bar{B}_\delta (\rho = R_\delta, \alpha, z = l_m/2 + l_b/2)\, \vec{e}_\rho$ is the radial air gap excitation flux density component effective for axial force generation. The average flux density magnitude $\bar{B}_\delta = f(w_m, w_\delta)$ is a function of the magnet width and the air gap width of the drive. It is only weakly dependent of the air gap radius R_δ, which can be neglected in many practical cases. The (instantaneous) axial force of coil number k acting on the stator yields

$$F_{c,k}^{(z)}(t) = k_F^c \left(N_c i_{c,k}\right) \,, \tag{27}$$

introducing the force-current coefficient of a single coil

$$k_F^c = 2\bar{l}_c \bar{B}_\delta (w_m, w_\delta) = 2R_\delta \Delta\gamma_c \,(1 - 2\alpha_0 - \alpha_c)\, \bar{B}_\delta (w_m, w_\delta) \,. \tag{28}$$

The total stator force of the air gap winding in axial direction $\vec{e}_z$ can thus be summarized as

$$F^{(z)} = \sum_{k=1}^{m} F_{c,k}^{(z)} = m k_F^c N_c i_F + k_F^c N_c \Re \left\{ \underline{i}_T^{dq} e^{j\nu_r^e} \underbrace{\sum_{k=1}^{m} e^{-j(k-1)p_r \Delta\gamma_c}}_{=0} \right\} = k_F N_c i_F \,. \tag{29}$$

Due to the three dimensional field geometry, the overall force-current coefficient $k_F = m k_F^c$ of the drive is preferably determined via finite element analysis software and/or by measurements on a test rig. The expression (29) is not dependent on the torque producing current component $\underline{i}_T^{dq}$ due to the usage of a set of m balanced, harmonic coil currents.

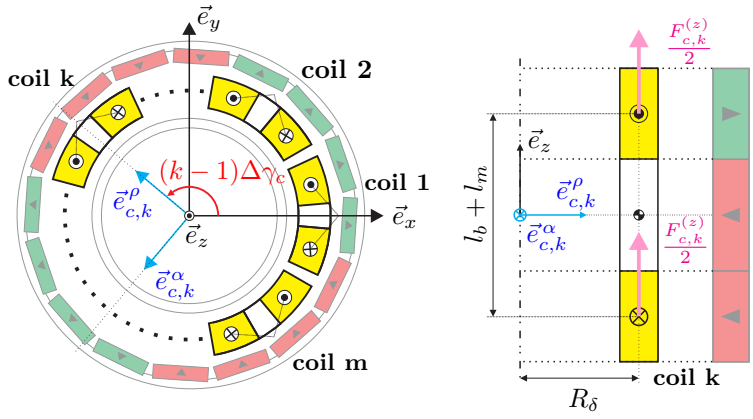

Figure 8: Generation of tilt torques caused by the coil end windings. Depicted rotor pole system $p_r = 2$.

7 Formal Description of the Rotor Tilt Torques

The point of force application of the coil end-windings do not match with the center of mass of the stator. Due to the special rotor magnetization pattern, the current excited stator coils may produce undesirable resulting tilt torques. It is therefore advisable to establish reliable relations to predict the appearance of tilt torques for specific drive configurations. Given is an air gap winding arrangement depicted in Figure 8 consisting of m non-overlapping air-core stator coils. It is assumed, that there are only minor displacements between the mass centers of stator and rotor. The winding system is supposed to be symmetrical, the single coils provide equal axial forces at equal coil currents, as the end windings exhibit equal average lengths. The tilt torque contribution acting on the stator caused by the end-windings of coil number k is covered by

$$\vec{t}_{c,k} = -R_\delta F^{(z)}_{c,k} \vec{e}^{\,\alpha}_{c,k} = -R_\delta k^c_F (N_c i_{c,k}) \vec{e}^{\,\alpha}_{c,k} \tag{30}$$

according to Figure 8. A special coil reference frame $\left(\vec{e}^{\,\rho}_{c,k}, \vec{e}^{\,\alpha}_{c,k}\right)$ in polar coordinates is defined to facilitate the mathematical treatment of multiple, angular displaced coils. Using the transformation

$$\vec{e}^{\,\alpha}_{c,k} = -\sin\left[(k-1)\Delta\gamma_c\right]\vec{e}_x + \cos\left[(k-1)\Delta\gamma_c\right]\vec{e}_y$$

between the reference frame of coil k and the cartesian stator reference frame, the resulting stator tilt torque vector of an air gap winding system consisting of m coils can be formulated as summation over all (m coils) contributions (30). Using the abbreviation

$$\varkappa = R_\delta k^c_F N_c\,, \tag{31}$$

the stator tilt torque vector can be stated as

$$\mathbf{t}^{xy}_{tilt} = \begin{bmatrix} t^x \\ t^y \end{bmatrix} = \varkappa \begin{bmatrix} \sum_{k=1}^m i_{c,k} \sin\left[(k-1)\Delta\gamma_c\right] \\ -\sum_{k=1}^m i_{c,k} \cos\left[(k-1)\Delta\gamma_c\right] \end{bmatrix}. \tag{32}$$

7.1 Influence of Axial Force Producing Current Components

The general expression (32) can be used to analyze the impact of axial force producing (zero sequence) coil current components $i_{c,k} = i_F$ on the tilt torque vector. The application of Euler's formula to the trigonometric summations in (32) and a subsequent utilization of the geometric series properties lead to

$$t^x = \varkappa \sum_{k=1}^{m} i_F \sin\big[(k-1)\Delta\gamma_c\big] = \varkappa i_F \frac{1}{2j}\left(\sum_{k=1}^{m} e^{j(k-1)\Delta\gamma_c} - \sum_{k=1}^{m} e^{-j(k-1)\Delta\gamma_c}\right) = 0 \tag{33}$$

$$t^y = 0\,. \tag{34}$$

If all the zero sequence coil current components of the considered air gap winding have equal magnitudes $i_{c,k} = i_F$, no resulting tilt torque is present during axial force generation.

7.2 Influence of Balanced, Harmonic Current Components

The generation of rotating field waves using polyphase winding structures requires a set of balanced, rotor angle dependent, harmonic coil current components

$$i_{c,k} = \hat{\imath}_T \cos\big[\varsigma - (k-1)p_s\Delta\gamma_c\big] \tag{35}$$

and $\varsigma = \nu_r^e + \varphi_i$. Those coil current components (usually drive torque producing) may also generate nonzero stator tilt torque vectors for certain drive configurations, which is subject of the present analysis. The substitution of the harmonic coil current component (35) into (32) leads to

$$\begin{aligned} t^x =& \varkappa \sum_{k=1}^{m} \hat{\imath}_T \cos\big[\varsigma - (k-1)p_s\Delta\gamma_c\big] \sin\big[(k-1)\Delta\gamma_c\big] \\ =& \frac{\varkappa}{2}\hat{\imath}_T \frac{1}{2j}\left(e^{j\varsigma} \sum_{k=1}^{m} e^{-j(k-1)(p_s-1)\Delta\gamma_c} - e^{-j\varsigma} \sum_{k=1}^{m} e^{j(k-1)(p_s-1)\Delta\gamma_c} \right. \\ & \left. - e^{j\varsigma} \sum_{k=1}^{m} e^{-j(k-1)(p_s+1)\Delta\gamma_c} + e^{-j\varsigma} \sum_{k=1}^{m} e^{j(k-1)(p_s+1)\Delta\gamma_c} \right) \end{aligned} \tag{36}$$

after using Euler's formula and a few algebraic transformations. The calculation of the $\vec{e}_y$-component of the stator tilt torque vector (32) can be effected likewise and will be suppressed at this point therefore. The resulting tilt torque expression takes the simple form

$$t^x = \begin{cases} \pm m\dfrac{\varkappa}{2}\hat{\imath}_T \sin(\nu_r^e + \varphi_i) & \text{if } p_s = mz \pm 1 \text{ and } z \in \mathbb{Z}; \\ 0 & \text{else.} \end{cases} \tag{37}$$

for the component $\vec{e}_x$ and

$$t^y = \begin{cases} -m\dfrac{\varkappa}{2}\hat{\imath}_T \cos(\nu_r^e + \varphi_i) & \text{if } p_s = mz \pm 1 \text{ and } z \in \mathbb{Z}; \\ 0 & \text{else.} \end{cases} \tag{38}$$

for the component $\vec{e}_y$. In general, rotor angle dependent tilt torque production is undesirable in Axial-Force/Torque Motors. The condition for a disappearing tilt torque vector can be stated as

$$\mathbf{t}_{tilt}^{xy} = 0 \qquad \text{if } \boxed{p_s \neq mz \pm 1} \text{ and } z \in \mathbb{Z}\,. \tag{39}$$

Table 2 is a representation of the wave numbers relevant for tilt torque generation dependent on the total number of coils m. If the ordinal wave numbers specified in Table 2 are also present in the corresponding column of the m.m.f. spectrum of Table 1, the desired drive configuration produces rotor angle dependent tilt torques according to (37) and (38).

	z	0	1	2	3	4	5	7	8	9
$m=4$	$p_s = mz+1$:	1	5	9	13	17	21	25	29	33
	$p_s = mz-1$:		3	7	11	15	19	23	27	31
$m=5$	$p_s = mz+1$:	1	6	11	16	21	26	31	36	41
	$p_s = mz-1$:		4	9	14	19	24	29	34	39
$m=6$	$p_s = mz+1$:	1	7	13	19	25	31	37	43	49
	$p_s = mz-1$:		5	11	17	23	29	35	41	47

Table 2: Conditions for rotor angle dependent tilt torque generation. If the specified ordinal wave numbers n are also present in the corresponding m.m.f. spectrum of Table 1, tilt torques are initiated by the drive torque coil currents.

8 Numerical Analysis of Axial-Force/Torque Motor Topologies

Various 3D finite element simulations have verified the developed analytical framework for polyphase Axial-Force/Torque Motor design. This section presents the numerical results for Bearingless Axial-Force/Torque Motors with an air gap winding consisting of $m=4$, $m=5$ and $m=6$ air-core coils and different rotor pole pair numbers.

Geometric data of the actuator: average air gap radius: $R_\delta = 25\,\text{mm}$, height of motor magnets: $l_m = 10\,\text{mm}$, mechanical gaps between winding and rotor $gap = 0.7\,\text{mm}$, magnet length: $w_m = 4\,\text{mm}$, air gap length: $w_\delta = 6\,\text{mm}$, copper filling factor $k_{cu} = 0.57$, maximum current density in copper: $S_{cu}^{RMS} = 15 A.mm^{-1}$, permanent magnet system: NdFeB N44SH.

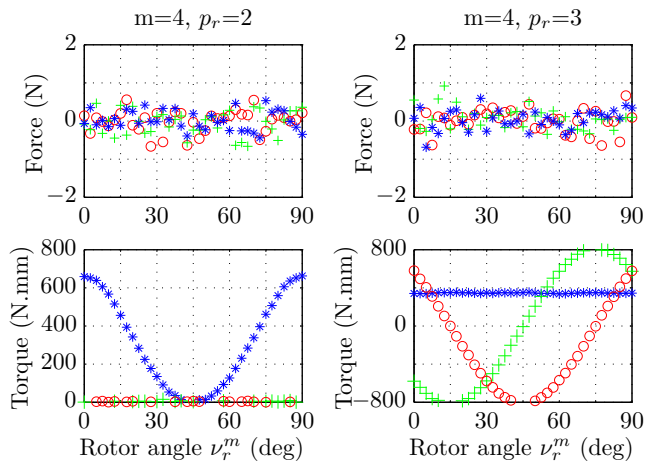

Figure 9: 3D fea results. Number of coils: m=4. Blue stars: drive torque T^z / axial levitation force F^z. Red circles: tilt torque t^x / radial force F^x. Green plus: tilt torque t^y / radial force F^y.

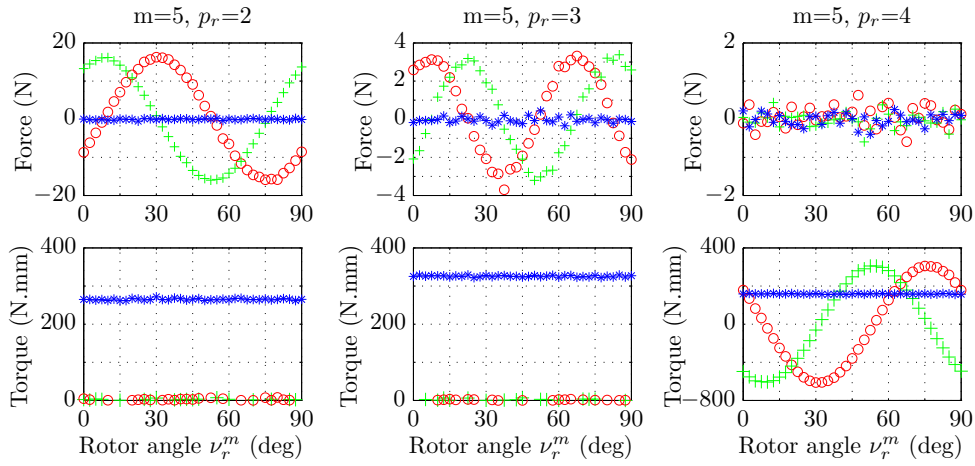

Figure 10: 3D fea results. Number of coils: m=5. Blue stars: drive torque T^z / axial levitation force F^z. Red circles: tilt torque t^x / radial force F^x. Green plus: tilt torque t^y / radial force F^y.

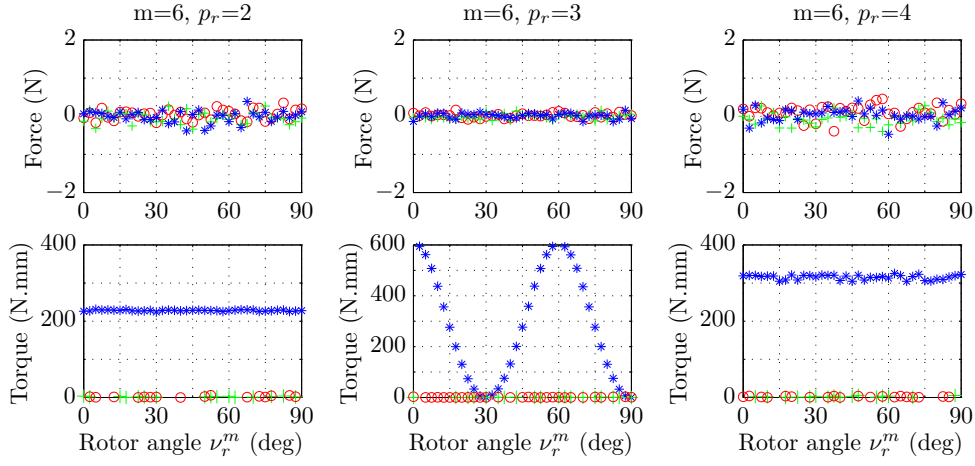

Figure 11: 3D fea results. Number of coils: m=6. Blue stars: drive torque T^z / axial levitation force F^z. Red circles: tilt torque t^x / radial force F^x. Green plus: tilt torque t^y / radial force F^y.

9 Conclusion

The presented results are valid for Lorentz-Force actuators with air gap windings and non-slotted stator and rotor elements. The analytical deductions are verified using numerical 3D finite element analysis. The next step in drive development will be the design of a new polyphase prototype, the experimental verification and the extension of the presented bearingless drive principle to slotted machine topologies.

Acknowledgment

The presented research work has been supported by the ACCM[1] GmbH, which is part of the COMET/K2 program of the Federal Ministry of Transport, Innovation and Technology and the Federal Ministry of Economics and Labour, Austria. The authors would like to thank all involved partners for their support in making this work possible.

References

[1] D. Schröder. *Elektrische Antriebe - Grundlagen, vol.1*. Springer-Verlag, Berlin, Heidelberg, 2007.

[2] G. Schweitzer and E. H. Maslen. *Magnetic Bearings: Theory, Design, and Application to Rotating Machinery*. Springer-Verlag, Berlin, Heidelberg, 2009.

[3] A. Chiba, T. Fukao, and O. Ichikawa. *Magnetic Bearings and Bearingless Drives*. Elsevier/Newnes, Amsterdam, London, 2005.

[4] Siegfried Silber. *Beiträge zum lagerlosen Einphasenmotor*. PhD thesis, Johannes Kepler University Linz, Austria, 2000.

[5] Herbert Grabner. *Dynamik und Ansteuerkonzepte lagerloser Drehfeld-Scheibenläufermotoren in radialer Bauform*. PhD thesis, Johannes Kepler University Linz, Austria, 2006.

[6] Wolfgang Gruber. *Untersuchungen zu lagerlosen Segmentmotoren*. PhD thesis, Johannes Kepler University Linz, Austria, 2009.

[7] Walter Bauer and Wolfgang Amrhein. Design and sizing relations for a novel bearingless motor concept. In *International Conference on Electrical Machines and Systems, ICEMS 2011, Beijing, China*, August 2011.

[8] Walter Bauer and Wolfgang Amrhein. Electrical design and winding selection for a bearingless axial-force/torque motor. In *International Symposium on Power Electronics, Electrical Drives, Automation and Motion, SPEEDAM 2012, Sorrento, Italy*, June 2012.

[9] Jacek F. Gieras, Chong Wang, and Joseph Cho Lai. *Noise of Polyphase Electric Motors*. CRC Press, Taylor & Francis Group, Boca Raton, 2006.

[10] Germar Müller and Bernd Ponick. *Theorie elektrischer Maschinen, 6. Auflage*. Wiley-VCH Verlag, Dresden, Hannover, 2008.

[1] Austrian Center of Competence in Mechatronics, `http://www.accm.co.at`